Symmetry-constrained reorganization of Dirac cones in topological insulators by surface modification

Guang Bian, Xiaoxiong Wang, Yang Liu, T. Miller, and T.-C. Chiang

Phys. Rev. B **84**, 235414 — Published 1 December 2011

DOI: 10.1103/PhysRevB.84.235414

Symmetry-Constrained Reorganization of Dirac Cones in Topological Insulators by Surface Modification

Guang Bian,[1,2] Xiaoxiong Wang,[3] Yang Liu,[1,2] T. Miller,[1,2] and T.-C. Chiang[1,2]

[1]*Department of Physics, University of Illinois at Urbana-Champaign,*

1110 West Green Street, Urbana, Illinois 61801-3080, USA

[2]*Frederick Seitz Materials Research Laboratory, University of Illinois at Urbana-Champaign,*

104 South Goodwin Avenue, Urbana, Illinois 61801-2902, USA

[3]*College of Science, Nanjing University of Science and Technology, Nanjing 210094, China*

PACS numbers: 71.70.Ej 73.20.At 73.21.Fg 79.60.Dp

ABSTRACT

Topological insulators possess a symmetry-protected surface spin current, a property highly relevant to spintronics applications. This current arises from gapless spin-polarized surface states. Calculations show that these states can undergo drastic transformations with surface treatment, despite the overall symmetry-based constraints. Specifically, the single Dirac cone at the zone center for the surface states in Bi_2Se_3 (Bi_2Te_3) is transformed, upon hydrogen termination, into three Dirac cones at the zone boundary. This trifurcation enhances the surface spin polarization, but leaves the overall topological order invariant.

I. INTRODUCTION

Topological insulators are a new class of materials characterized by a bulk band gap, a strong spin-orbit coupling, and a conducting surface.[1-8] In these materials, an odd number of spin-polarized surface states span the bulk gap, giving rise to a net surface spin current at the Fermi level.[9-11] This spin current, protected by bulk symmetry, is of great interest for applications involving spin information processing.[12,13] While the topological order is a robust quantity, the topological surface states themselves giving rise to the spin current are not necessarily robust and can be highly sensitive to the boundary conditions.[14,15] This is a concern, as actual utilization of these materials requires a stable structure, and surface passivation, capping, or interface formation is generally required for device architecture. How this topological invariance manifests itself upon surface modification is an issue of importance to the basic physics of this class of material and the actual implementation for application. Our work is a demonstration of a drastic transformation of the topological surface states in a model system under the constraint of topological-order invariance. Specifically, the surface states of Bi_2Se_3 and Bi_2Te_3 form a single Dirac cone at the zone center $\bar{\Gamma}$.[16-18] First-principles calculations based on a slab geometry show that, upon hydrogen termination of either face of the slab, the Dirac cone associated with this face is replaced by three Dirac cones centered at the time-reversal-invariant $\bar{M}$ points at the zone boundary, yet the topological order remains the same as evidenced by detailed calculations of the wave functions. Furthermore, the topological surface states on the two faces of the slab, with or without hydrogen termination, are quantum-mechanically entangled, and the overall topological order of the system must be analyzed within this context.

An often-invoked argument for the robustness of the surface spin current in topological

insulators is that the spin-polarized surface states have a vanishing back scattering probability by surface perturbations because of time-reversal symmetry; indeed, experiments have demonstrated the insensitivity of the surface state Dirac cones to adsorption or gas exposure.[14,19,20] More generally, though, the surface spin texture can be affected by spin-orbit coupling through altered electronic orbital motions upon surface modification, and it is not necessarily an invariant quantity. Specifically, hydrogen termination leads to surface passivation by saturation of surface dangling bonds. Both the orbital and spin degrees of freedom of the surface electrons can be substantially altered, as demonstrated herein for Bi_2Se_3 and Bi_2Te_3. The results suggest interesting possibilities for optimizing material properties or device performance.

II. COMPUTATIONAL METHODS

Our first-principles electronic structure calculations are performed under the local-density approximation within the density functional theory framework using HGH-type pseudopotentials and a plane-wave basis set; the program is based on the ABINIT algorithm including spin-orbit coupling.[21,22] The lattice constants of Bi_2Se_3 and Bi_2Te_3 are adopted from previous studies.[23,24] Calculations for the bulk materials establish the bulk band edges. Calculations for a (111) slab geometry for various thicknesses up to 12 quintuple layers (QLs), where 1 QL = 9.55 Å for Bi_2Se_3 and 10.16 Å for Bi_2Te_3, yield surface states and quantum well states; the surface states are well converged by ~4 QLs. The bond lengths of H-Se and H-Te for hydrogen-terminated surfaces are determined to be 1.46 and 1.69Å, respectively.

III. RESULTS AND DISCUSSION

A. Reorganization of Dirac cones in topological insulators by hydrogen termination

The band dispersion relations for 6 QL freestanding Bi_2Se_3 and Bi_2Te_3 slabs are presented as solid curves in Figs. 1(a) and 1(b), respectively. The shaded areas represent the projected bulk band regions; these results are in good agreement with previous calculations where available.[23,24] The dashed horizontal lines indicate the midgap positions, or the bulk Fermi levels. The fundamental band gaps are 0.35 and 0.16 eV, respectively. In each case near the zone center $\bar{\Gamma}$ are two surface bands that span the gap and cross each other at $\bar{\Gamma}$ to form a Dirac cone. The Dirac cone has a left-handed helical spin texture,[16] and the two surface bands have opposite spin polarizations. Each point on the surface bands, except the Dirac point, is doubly degenerate corresponding to the surface states located on the two opposite faces of the slab, which are related by space inversion and time reversal. The two surface bands are shown in red and blue color to highlight their different spin orientations. They disperse into the bulk continuum a short distance away from $\bar{\Gamma}$, where they lose their surface character and become quantum well states.[25] Each band remains doubly degenerate; the two surface states associated with the two faces of the slab now fully penetrate the film and combine to form a spin-degenerate pair of quantum well states.[26] Each quantum well subband is spin degenerate as required by space inversion symmetry.

Results from calculations for the same slab with the bottom face of the slab terminated by hydrogen are presented in Figs. 1(c) and 1(d). While the surface bands near the zone center remain unchanged, a new Dirac cone emerges at $\bar{M}$, and these two cones are smoothly

connected throughout the surface zone. With the newly emerged Dirac cone, the total number of surface band crossings of the bulk Fermi level between $\overline{\Gamma}$ and $\overline{M}$ becomes an even number (two or four). This is contrasted by a single crossing for the case without the hydrogen. As is well established, topological insulators must have an odd number of such crossings. At first glance, our results would seem to violate the topological order of the system, which is a bulk property and cannot be altered by hydrogen termination.

This puzzling behavior is clarified by considering slabs with both faces terminated by hydrogen. The results, shown in Figs. 1(e) and 1(f), reveal the same surface bands associated with the Dirac cone at $\overline{M}$, while the surface bands associated with the Dirac cone at $\overline{\Gamma}$ are eliminated. The number of Fermi level crossings is again odd. Evidently, the Dirac cone at $\overline{M}$ is associated with the hydrogen-terminated face, while the Dirac cone at $\overline{\Gamma}$ is associated with the bare face. For the slab with just one face terminated, both sets of surface bands appear in the calculation. The counting of the Fermi level crossing for each face of the slab is still consistent with the topological order. There are three symmetry-equivalent $\overline{M}$ points in the first zone, thus, hydrogen-termination results in a trifurcation of the Dirac cone. Hydrogen-termination also breaks the inversion symmetry of the system. The spin degeneracy of each quantum well subband is lifted,[27] resulting in a small energy splitting, which diminishes with increasing slab thickness. This splitting is evident for some of the bands in Figs. 1(c) and 1(d), but not seen in the symmetrical cases.

The plane-averaged charge densities of the two surface bands are presented in Figs. 2(b) and 2(c) for a 12-QL Bi_2Se_3 slab with its bottom face terminated by hydrogen; the results are

presented for 11 equally spaced points between $\bar{\Gamma}$ and $\bar{\mathrm{M}}$ as indicated by the triangles in Fig. 2(a). The vertical dashed lines in Figs. 2(b) and 2(c) indicate the QLs. The two surface states, labeled α and β, are degenerate at $\bar{\Gamma}$ and pinned at the top face of the slab. Near $k_x = 0.1\left|\bar{\Gamma}\bar{\mathrm{M}}\right|$, state β grazes the bulk valence band edge and develops a charge density more akin to a bulk state. It then evolves, at larger k_x, back into the band gap, and the associated charge density becomes pinned at the bottom face all the way to $\bar{\mathrm{M}}$. State α shows a similar migration of charge density from the top face to the bottom face, but the transition occurs in a different range in *k* space. The directions of the triangles in Fig. 2(b), up- and down-pointing, indicate charge localization near the top and bottom faces of the slab, respectively.

This migration of charge density for each state can be described quantitatively by the charge localization function

$$C(k_x) = \frac{2}{D}\langle \psi(k_x)|z|\psi(k_x)\rangle,$$

where *D* is the film thickness, and *z* is the normal coordinate of the slab with its origin at the midpoint of the slab. This quantity ranges from –1 to +1, corresponding to a charge distribution fully concentrated at the bottom and top faces, respectively. The results, presented in Fig. 3(a), show a rapid passage around the places where the two states graze the bulk band edges.

The spin polarization of the two surface states α and β are characterized by the expectation values of the spin operators. Presented in Fig. 3(b) is $\langle S_y \rangle$ normalized to $\hbar/2$. Our calculations yield $\langle S_x \rangle = \langle S_z \rangle = 0$ (*x* points along $\bar{\Gamma}\bar{\mathrm{M}}$, and *z* points along the surface normal). The two states are thus strictly polarized along –*y* and +*y*, respectively, in accordance with the Rashba interaction,[28] and the directions of spin polarization are maintained throughout the charge

migration from the top to the bottom faces. These spin-locked channels allow the two faces of the slab to communicate. The magnitude of the spin polarization, normalized to $\hbar/2$, is less than 100% because of the coupling of the spin and orbital degrees of freedom.[15,26] It is about 50%~60% near $\overline{\Gamma}$ where these states are associated with the bare top face of the slab, and it increases to almost 80% near $\overline{\mathrm{M}}$, where they become surface states associated with the hydrogen-terminated bottom face. Evidently, hydrogen termination enhances the spin polarization of the surface states by partly disentangling the spin and orbital degrees of freedom.

The hydrogen-induced reorganization of the Dirac cones, from one cone at $\overline{\Gamma}$ to three cones at $\overline{\mathrm{M}}$, as well as the formation of the spin-locked (or quantum-mechanically entangled) channels, can be understood qualitatively using the schematic diagram in Fig. 4(a). To first order, surface adsorption shifts the overall crystal potential for the surface states. With increasingly stronger interaction, the Dirac cone is shifted out of the band gap (middle panel), and eventually the displaced surface bands can intersect again in the gap at the zone boundary $\overline{\mathrm{M}}$ point, resulting in a new Dirac cone there (bottom panel). If the band movement can be adjusted, the system could potentially adopt a configuration with gapless surface states but no Dirac cones in the bulk gap, as indicated in the middle panel of Fig. 4(a). With just one face of the slab terminated by hydrogen, the surface states on the two faces must connect via avoided crossings through bulk-like states that are located just at the bulk band edges, as indicated in Fig. 4(b). The quantization of the bulk states into quantum-well-state pairs in films helps isolate the spin-locked surface bands from the bulk-derived states.

B. Evolution of the band structure upon varying the hydrogen atom position

If the hydrogen atoms are gradually moved from a large distance away to their final equilibrium adsorption positions on both faces of a Bi_2Se_3 slab, the band structure should evolve smoothly from one configuration to the other. The results for several selected H-Se bond lengths for symmetric H adsorption on a 6 QL Bi_2Se_3 slab are shown in Fig. 5.

When the bond length is large, the band structure of the slab is not affected by the hydrogen as shown in Fig. 5(a). With the hydrogen atoms approaching the surfaces, the original Dirac point at the zone center moves downwards in energy, and eventually merges into the valence band region. Band α, however, remains pinned within the bulk band gap because of anticrossing. The portion of the band near $\overline{\Gamma}$ begins to graze the valence band edge, and the portion of the band near the $\overline{\mathrm{M}}$ point, originally grazing the conduction band edge, now moves down into midgap. Time-reversal symmetry (Kramers theorem) requires double degeneracy at the $\overline{\mathrm{M}}$ point, and this requirement is satisfied by state α dragging its companion quantum well subband into the band gap to form a new surface band β'. The pair α and β' forms a Dirac cone at $\overline{\mathrm{M}}$ for the hydrogen-terminated surface.

C. Hydrogen-induced bonding states below the *p* valence bands

In addition to modifying the gapless surface states, hydrogen adsorption gives rise to new surface states within bulk band gaps. A prominent example is seen in Fig. 5 where two H-induced surface bands, α_H and β_H, arise within the *s*-*p* gap (the lower *s* bands are not shown). This pair shows the usual Rashba splitting and is topologically trivial. Presented in Fig. 6 are the charge distributions of states α_H and β_H at $\overline{\Gamma}$ for a 12 QL Bi_2Se_3 slab with its

bottom face terminated by H. The charges are strongly localized near the H-Se bonds. The calculated spin polarizations of these states are nearly 100%.

D. Robustness of the first-principles results

The calculations described in the main text were performed using LDA. To test the robustness of the results, we show in Figs. 7(a) and 7(b) the calculated dispersion relations for a 6 QL slab of Bi_2Se_3 with its bottom face terminated by hydrogen using two different exchange-correlation functionals: LDA and Perdew-Burke-Ernzerhof GGA, respectively. In each case, the H atom position is optimized energetically. The results are nearly identical; the main difference is that the Dirac point is at a slightly different energy. We have also explored the issue of atomic relaxation by allowing the positions of the surface layer of Bi_2Se_3 and the H atoms to relax in the LDA calculation. We find that the Se atom adjacent to each H atom moves outwards by 0.01 Å and the length of the H-Se bond is elongated by 0.05 Å. These slight atomic movements are not expected to cause significant changes in the calculated band structure. Indeed, the results, presented in Fig. 7(c), are very close to those in Figs. 7(a) and 7(b). Specifically, the topological properties of the system remain the same. Thus, our conclusions are independent of the details of the calculation.

IV. CONCLUDING REMARKS

Our work thus demonstrates that the surface states of topological insulators as well as their associated spin structure and degree of spin polarization can be substantially modified by surface and/or interface engineering. The reconfigured surface states still satisfy the requirements of

topological order and time-reversal symmetry. Robustness of the surface states against surface perturbation because of a vanishing back scattering probability does not prevent these states from transforming into drastically different configurations. These conclusions are independent of the details of the model as demonstrated by additional calculations using the GGA approximation or allowing surface atomic layer relaxation. Our findings suggest opportunities for optimization of the spin current and spin texture. For thin films in the ballistic transport regime, the spin currents of the two opposite faces of the film could be connected with locked spin directions through bulk-like states without going through the side faces. This connection is a unique feature of topological insulators.

ACKNOWLEDGMENTS

We thank L. Fu and C.-K. Chiu for helpful discussions. This work is supported by the U.S. Department of Energy (grant DE-FG02-07ER46383). X. W. acknowledges financial support by the China Scholarship Council and the Young Scholar Plan of NJUST.

REFERENCES

[1] M. Z. Hasan and C. L. Kane, Rev. Mod. Phys. **82**, 3045 (2010).

[2] X. L. Qi and S. C. Zhang, Rev. Mod. Phys. **83**, 1057 (2011).

[3] J. E. Moore and L. Balents, Phys. Rev. B **75**, 121306 (2007).

[4] B. A. Bernevig, T. L. Hughes and S.-C. Zhang, Science **314**, 1757 (2006).

[5] C. L. Kane and E. J. Mele, Phys. Rev. Lett. **95**, 226801 (2005).

[6] S. Murakami, N. Nagaosa and S.-C. Zhang, Phys. Rev. Lett. **93**, 156804 (2004).

[7] X.-L. Qi and S.-C. Zhang, Phys. Today **63**, 33 (2010).

[8] M. König *et al.*, Science **318**, 766-770 (2007).

[9] D. Hsieh *et al.*, Nature **452**, 970 (2008).

[10] L. Fu and C. L. Kane, Phys. Rev. B **76**, 045302 (2007).

[11] R. Roy, Phys. Rev. B **79**, 195322 (2009).

[12] I. Garate and M. Franz, Phys. Rev. Lett. **104**, 146802 (2010).

[13] L. Fu and C. L. Kane, Phys. Rev. Lett. **100**, 096407 (2008).

[14] Y. L. Chen *et al.*, Science **329**, 659 (2010).

[15] O. V. Yazyev, J. E. Moore and S. G. Louie, Phys. Rev. Lett. **105**, 266806 (2010).

[16] Y. Xia *et al.*, Nat Phys **5**, 398 (2009).

[17] Y. L. Chen *et al.*, Science **325**, 178 (2009).

[18] Y. Zhang *et al.*, Nat Phys **6**, 584 (2010).

[19] H. M. Benia, C. Lin, K. Kern and C. R. Ast, arXiv:1105.2664v1 (2011).

[20] Z.-H. Pan, D. R. Gardner, S. Chu, Y. S. Lee and T. Valla, arXiv:1104.0966v1 (2011).

[21] X. Gonze *et al.*, Comp. Mater. Sci. **25**, 478 (2002).

[22] X. Gonze *et al.*, Zeit. Krist. **220**, 558 (2005).

[23] Z. Wei *et al*., New J. Phys. **12**, 065013 (2010).

[24] H. Zhang *et al.*, Nat Phys **5**, 438 (2009).

[25] T. C. Chiang, Surf. Sci. Rep. **39**, 181 (2000).

[26] G. Bian, T. Miller and T.-C. Chiang, Accepted by Phys. Rev. Lett. **107**, 036802 (2011).

[27] J. H. Dil *et al.*, Phys. Rev. Lett. **101**, 266802 (2008).

[28] Y. A. Bychkov and J. Rashba, Phys. C: Solid State Phys. **17**, 6039 (1984).

FIG. 1 (color online). (a and b) Calculated dispersion relations (solid curves) for 6 QL slabs of Bi_2Se_3 and Bi_2Te_3, respectively. The shaded areas are projected bulk band regions. The horizontal dashed lines indicate the bulk Fermi levels. The red and blue curves represent surface states and their continuations into the bulk regions. (c and d) Results after the bottom faces of the slabs are terminated by hydrogen. (e and f) Results after both faces are terminated by hydrogen.

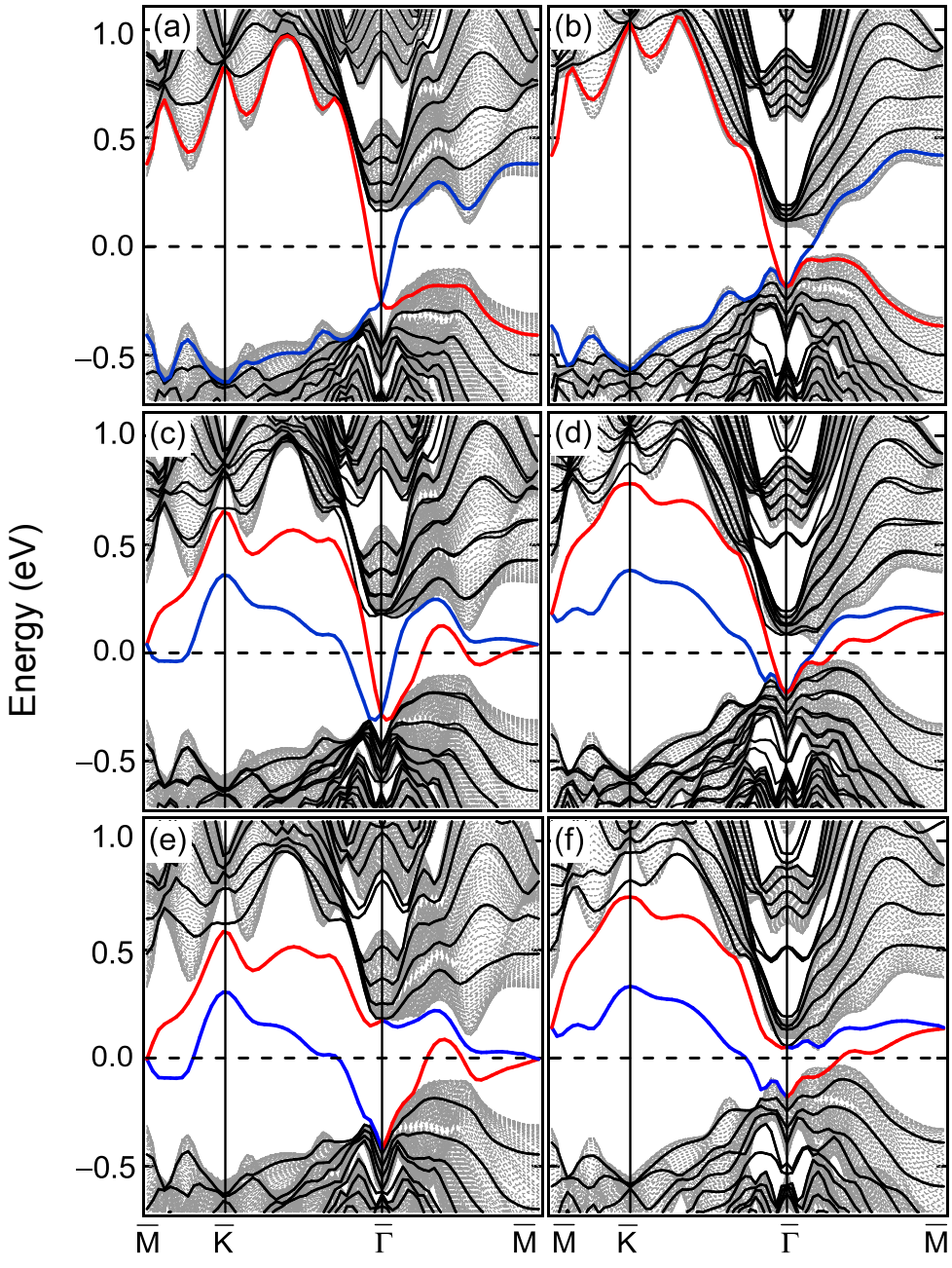

FIG. 2 (color online). (a) Surface bands, α and β, of a 12 QL slab of Bi_2Se_3 with its bottom face terminated by hydrogen. (b and c) Plane-averaged electronic charge densities for the two states.

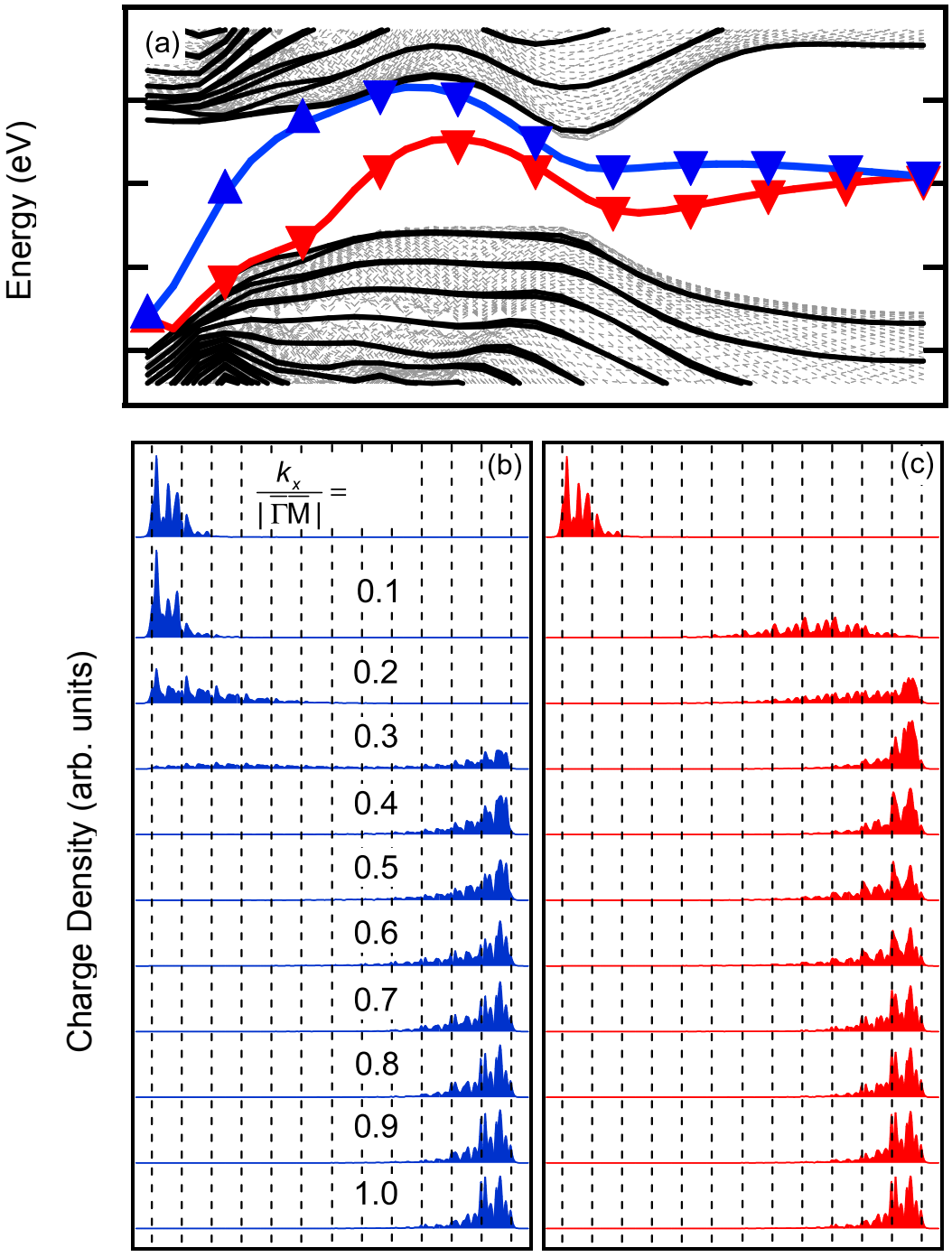

FIG. 3 (color online). (a) Charge localization as a function of k_x (along $\overline{\Gamma}\overline{\mathrm{M}}$) for the two states α and β in a 12 QL slab of Bi_2Se_3 with its bottom face terminated by hydrogen. It equals +1 and –1 for charge fully localized at the top and bottom faces of the slab, respectively. (b) Calculated spin polarization $2\langle S_y \rangle/\hbar$.

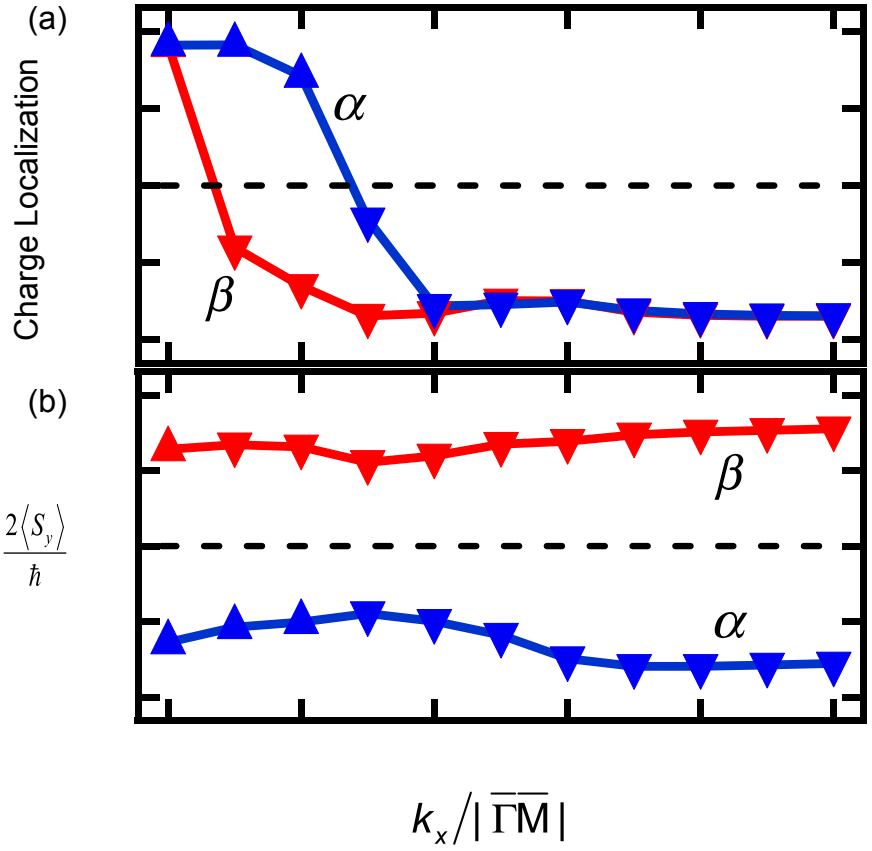

FIG. 4 (color online). (a) Displacement of Dirac cones in the vertical direction relative to the bulk conduction band (CB) and valence band (VB) as the surface potential changes. (b) The top two diagrams correspond to semi-infinite substrates, one without and the other with hydrogen termination; the Dirac cones are located at $\overline{\Gamma}$ and $\overline{M}$, respectively. For a finite slab with just the bottom face terminated by hydrogen, the Dirac cones associated with the two faces must connect by analytic continuation (or anti-crossing), resulting in spin-locked channels as shown in the bottom diagram.

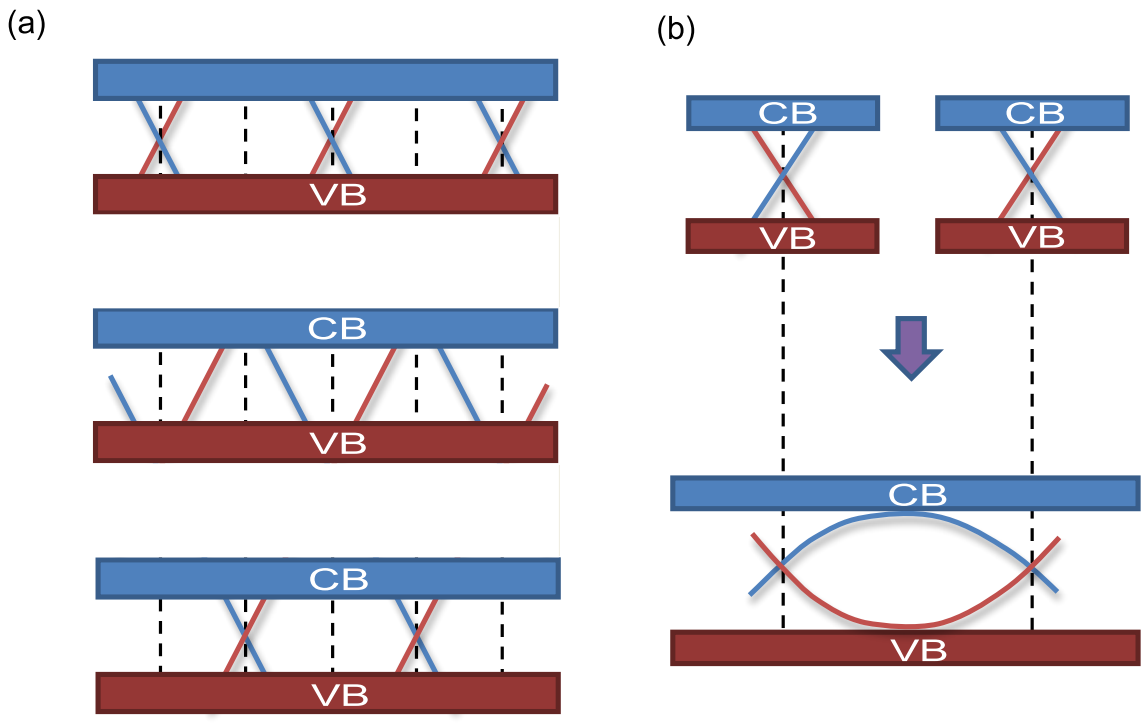

FIG. 5 (Color online). Evolution of band structure as hydrogen adatoms approach both faces of a 6 QL Bi_2Se_3 slab. The H-Se bond length is (a) ∞, (b) 3.00, (c) 1.91, and (d) 1.46 Å (equilibrium bond length).

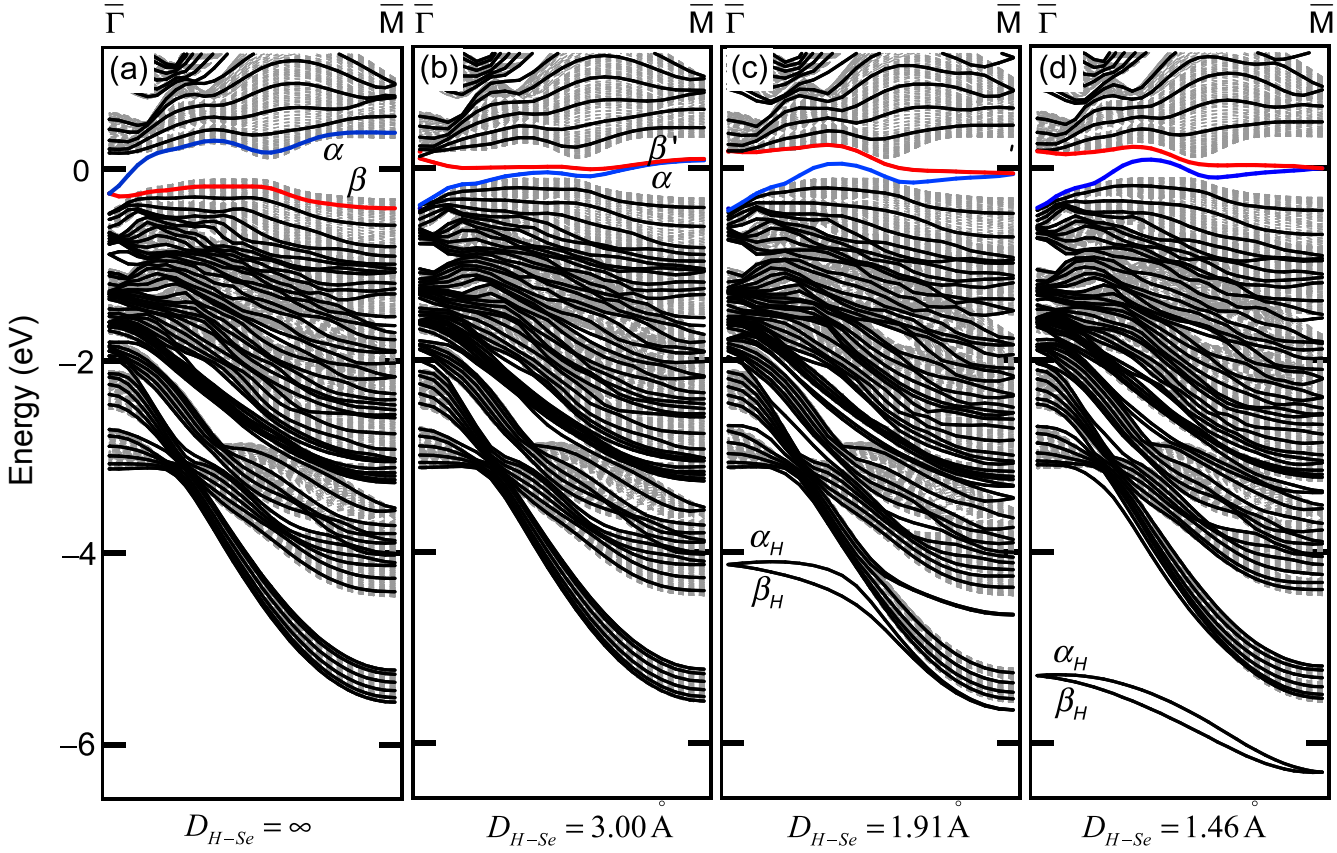

FIG. 6 (Color online). (a) Hydrogen-termination-induced bands α_H and β_H for a 12 QL Bi_2Se_3 slab with its bottom face terminated by H. (b) Charge distributions of states α_H and β_H at the zone center $\bar{\Gamma}$.

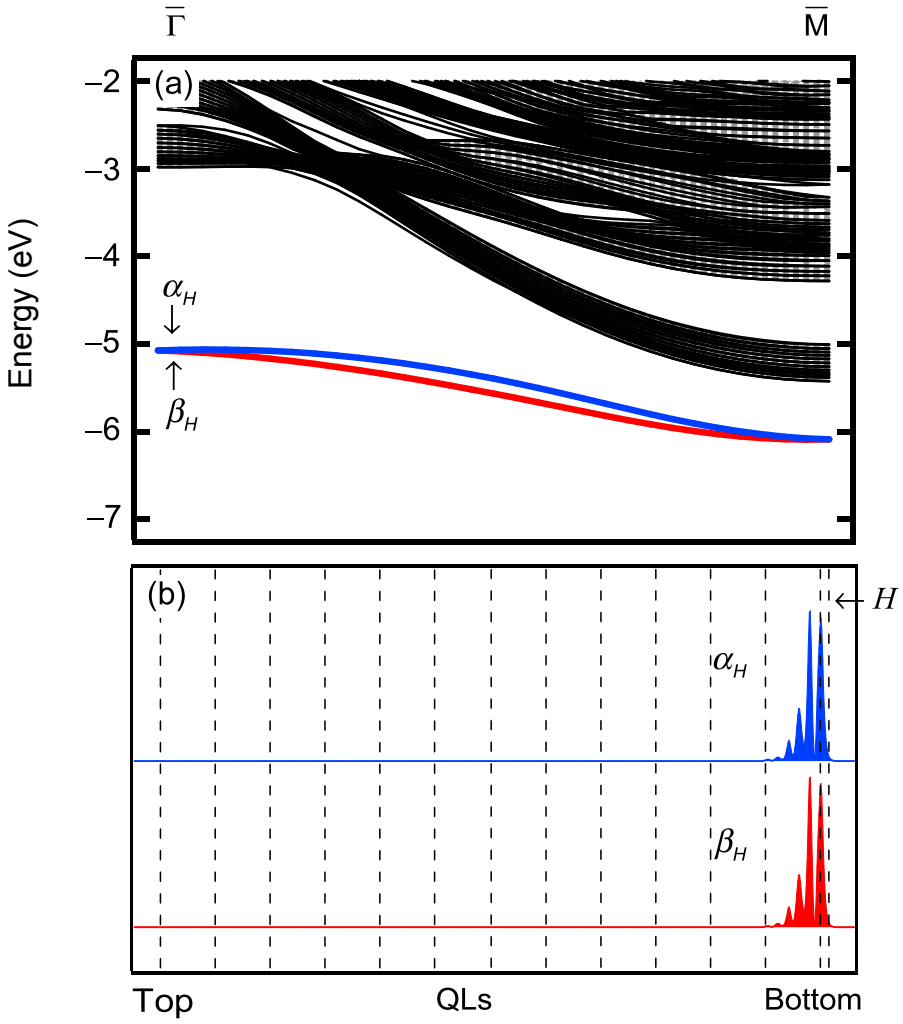

FIG. 7 (Color online). Calculated dispersion relations for a 6 QL slab of Bi_2Se_3 with its bottom face terminated by hydrogen. Only the position of the H atom is optimized using (a) LDA and (b) GGA for the exchange-correlation functional. (c) The surface Se atomic layer of Bi_2Se_3 and the H atoms are relaxed using LDA.